Journal of Inorganic and Organometallic Polymers and Materials (2023) 33:159–169
https://doi.org/10.1007/s10904-022-02493-9

RESEARCH

Influence of Synthesis Method on Structural, Morphological, Magnetic, and Antimicrobial Properties of Fe-Ag Nanoparticles

Sandrine Kamdoum Noukelag[1,2,3] · Maxwell Mewa-Ngongang[4,7] · Siphelo Ngqoloda[1] · Lebogang Kotsedi[2,3] · Lovasoa Christine Razanamahandry[5] · Seteno K. O. Ntwampe[6] · Christopher J. Arendse[1] · Malik Maaza[2,3]

Received: 8 August 2022 / Accepted: 3 September 2022 / Published online: 21 September 2022

Abstract
This contribution reports on the development of two versatile and efficient methods, namely the green and gamma radiolysis for Fe-Ag nanoparticles (NPs) synthesis, characterization, and further their growth inhibition potential on some spoilage microorganisms. Green Ag/Fe_2O_3 NPs were obtained at Fe-Ag [3:1], annealing temperature of 800 °C for 2 h, and gamma irradiated Ag/Fe_3O_4 NPs were obtained at Fe-Ag [7:1], a 50 kGy dose. The characterization techniques were performed with these two samples whereby the sizes from crystallographic and microscopic analyses were 39.59 and 20.00 nm for Ag/Fe_2O_3 NPs, 28.57 and 15.37 nm for Ag/Fe_3O_4 NPs, respectively. The polycrystallinity nature observed from X-ray diffraction was in accordance with the selected area electron diffraction. The vibrational properties confirmed the presence of bimetallic Fe-Ag NPs with the depiction of chemical bonds, Fe–O and Ag–O from attenuated total reflection-Fourier transform infrared spectroscopy and elements Ag, Fe, O from energy-dispersive X-ray spectroscopy analyses. The magnetic properties carried out using a vibrating sample magnetometer suggested a superparamagnetic behavior for the Ag/Fe_2O_3 NPs and a ferromagnetic behavior for the Ag/Fe_3O_4 NPs. Overall, the green Ag/Fe_2O_3 NPs successfully inhibited the growth of spoilage yeasts *Candida guilliermondii*, *Zygosaccharomyces fermentati*, *Zygosaccharomyces florentinus*, and spoilage molds *Botrytis cinerea, Penicillium expansum*, *Alternaria alstroemeriae*.

Keywords *Rosmarinus officinalis* leaves · Gamma radiolysis · Nanoparticles · Magnetic behavior · Antimicrobial

1 Introduction

Yeasts have traditionally been employed to manufacture alcoholic beverages, biomass, and other value-added chemicals and food products. They have numerous applications in food and beverage production, such as sausage, cheese, bakery products, and other fermented foods production [1]. However, spoilage yeasts contaminate these foods that have been processed and packaged, resulting in a significant impact on the agri-food industry. This is largely due to the poor handling, and processing including transportation facilities available to producers [2]. Some scholars reported that the yeasts, *Dekkera bruxellensis*, *Dekkera anomala*, *Zygosaccharomyces bailii*, *Hanseniaspora uvarum*, *Candida*

✉ Sandrine Kamdoum Noukelag
sandrinedoum@yahoo.fr

1 Department of Physics and Astronomy, University of the Western Cape, Robert Sobukwe Road, Private Bag X17, Bellville 7535, South Africa

2 UNESCO-UNISA Africa Chair in Nanosciences & Nanotechnology Laboratories (U2AC2N), College of Graduate Studies, University of South Africa (UNISA), Muckleneuk Ridge, PO Box 392, Pretoria, South Africa

3 Material Research Department (MRD), Nanosciences African Network (NANOAFNET), iThemba LABS-National Research Foundation, 1 Old Faure Road, Somerset West, PO Box 722, Somerset West 7129, Western Cape, South Africa

4 Bioresource Engineering Research Group (BioERG), Cape Peninsula University of Technology, PO Box 652, Cape Town 8000, South Africa

5 Economic Integration Division, African Union Development Agency, PO Box 1685, Johannesburg, South Africa

6 Center of Excellence in Carbon-Based Fuels, School of Chemical and Minerals Engineering, North-West University, Private Bag X1290, Potchefstroom 2520, South Africa

7 Post-Harvest and Agro-Processing Technologies, ARC Infruitec-Nietvoorbij (The Fruit, Vine and Wine Institute of the Agricultural Research Council), Private Bag X5026, Stellenbosch 7599, South Africa

guilliermondii, *Zygosaccharomyces fermentati*, *Schizosaccharomyces pombe, Debaryomyces hansenii, Saccharomyces cerevisiae,* and *Zygosaccharomyces florentinus*, are responsible for final product spoilage, and are sources of foodborne diseases [3–6]. This culminates in economic losses [7], noticeable in populated countries such as China, India, USA, Russia, and Nigeria.

Molds and fungi are distinguishable from other organisms by the formation of hyphae (a mass of branching, tangled filaments) that result in colony development. They grow on the food's surface and proliferate in beverages under conditions whereby there is sufficient dissolved oxygen and a suitable pH. These species, i.e., *Botrytis, Rhizopus*, *Colletotrichum*, *Alternaria*, *Fusarium*, *Penicillium*, *Aspergillus,* and *Monilinia*, sp., are commonly responsible for fruit, vegetable, beverage, and food spoilage [8–10]. *Botrytis* sp. are the primary spoilage organisms of many agriculturally important crops, including grape berries, tomato fruits, bulb flowers, and ornamental crops among others. If ingested, they inculcate negative clinical outcomes in humans [11]. According to the World Health Organization (WHO), 600 million diseases resulting in 420,000 deaths are annually reported worldwide due to these spoilage microorganisms [12]. As this is a concern, there needs to be alternative solutions to such a problem, as chemical preservatives have also been determined to be detrimental to human health [13]. It was also proven that the use of antibiotics against spoilage microorganisms is inefficient, and they have effects on the human body associated with severe clinical risks [14]. As such, some researchers found that the problem could be remediated by using nanoparticles (NPs), particularly Ag-based NPs, as antimicrobial agents in food decontamination and as deactivators of toxins [15]. They do assist in the generation of reactive oxygen species (ROS), which damage the spoilage organism's cell membranes via lysis, cytoplasmic contents deactivation, and disruption of cellular homeostasis, culminating in the preservation of edible goods, thus safe food, fruit, and beverages for consumers [16].

NPs with a combined Fe-Ag (iron-silver) crystalline matrix can enhance their appeal for application in the food industry as they can largely be recovered, i.e., due to the Fe components in their atomic structure, to minimize ingestion with Fe-Ag decontaminated food, fruit, and beverages [17]. Similarly, other properties such as recoverability due to magnetism have resulted in researchers conducting studies with bimetallic NPs consisting of Fe atoms [18]. Such NPs are hypothesized to possess higher efficacy in their intended application, and potential recovery or reuse, due to their synergistic effects and distinct properties, including their unique surface chemistry, small size, magnetism, and composition [19]. Therefore, bimetallic Fe-Ag NPs have been considered as suitable NPs for reducing food contamination, and deactivation of toxins due to their perceived antimicrobial activity against many microorganisms (bacteria, yeasts, fungi, viruses). This is due to their ability to generate ROS, its bandgap, stability, novel physicochemical, biological, and magnetic properties, all of which are imparted by characteristics associated with the induction of oxygen vacancies, crystalline transformation, and light scattering pattern alterations that make them different from their counterparts, albeit with inherent oxidation vulnerabilities [14, 15, 17].

The conventional synthesis methods employed to generate such NPs present some limitations, such as the overall synthesis cost, efficacy, high-temperature usage thus high energy consumption, particularly when high vacuum systems are used to decontaminate harmful by-products during synthesis [20–22]. Residual waste generated from such a synthesis process contributes to environmental problems associated with their disposal. To palliate such drawbacks, interest has been focused on the development of one-pot, less harmful, facile, cheap, reliable, and eco-friendly synthesis protocols by using nontoxic solvents and reagents under mild conditions. The aim is to largely produce the desired NPs whereby the size, shape, and morphology can be controlled, with supplementary attributes such as the inhibition of spoilage microorganisms for human health concerns [23–25]. Notably, for such synthesis, high-energy gamma Co^{60} ray irradiation is considered as an effective method for the synthesis and modification of nanomaterials due to several benefits such as (1) the reduction of metal ions to zero-valent metal particles under ambient conditions with minimized use of reducing agents; (2) the ability to control the rate of reduction reaction; (3) large-scale production potential that can be favorably set up with satisfactory requirements of a clean production process [26, 27]. Furthermore, producing NPs with a green synthesis method using plant extracts whereby the approach is performed without the use of chemicals (acid or base, surfactants, and solvents), generating a limited amount of waste with few by-products, further characteristics can be imparted onto the NPs due to residues of the biomolecules or organic elements in the plant extracts being embedded, i.e., additional properties associated with the enhanced immune system and blood circulation, the memory including cognitive stimulation, etc., in the final NPs [25, 28]. This is the case with NPs synthesis using some plant extracts such as *Alstonia Scholaris*, *Crataegus pinnatifida*, *Passiflora edulis*, *Euphorbia peplus*, *Amaranthus blitum*, *Adotha vasica*, *Eryngium planum*, *Argemone-mexicana*, *Vitis labrusa*, [17, 19, 29–35]. To the best of our knowledge, there is no finding thus regarding the synthesis of bimetallic Fe-Ag using *Rosmarinus officinalis* (rosemary) plant extract [36–38]. This study aims to report for the first time the different properties exhibited by green and gamma irradiated Fe-Ag NPs and their efficacy in inhibiting *Candida guilliermondii*, *Zygosaccharomyces fermentati*, *Zygosaccharomyces florentinus*, *Botrytis cinerea*, *Penicillium*

expansum, and *Alternaria alstroemeriae*, i.e., organisms associated with fruit, vegetable, beverage, and food spoilage.

2 Materials and Methods

2.1 Materials

Rosemary leaves (RL) were purchased from Western Cape Province-South Africa. Silver nitrate ($AgNO_3$), iron (III) chloride hexahydrate ($FeCl_3.6H_2O$), ferrous sulphate ($FeSO_4.7H_2O$), isopropyl alcohol ($CH_3CHOHCH_3$), and sodium hydroxide (NaOH) were purchased as analytical grade reagents (Sigma Aldrich, Modderfontein, Johannesburg, South Africa), and used without any further purification.

2.2 Methods

2.2.1 Preliminary Works

From research performed in a basic medium, no bimetallic Fe-Ag NPs were obtained at volume ratios [1:1], [2:1], [2:3], and [4:1]; annealing temperatures of 500 and 800 °C; including 4 and 2 g of RL using the green synthesis method. Similarly, for the gamma radiolysis approach performed at 50 kGy doses for all samples, no bimetallic Fe-Ag NPs were obtained as well at volume ratios [1:1], [2:1], [3:1], [4:1], [5:1], and [6:1].

2.2.2 Synthesis of Fe-Ag [3:1] via *an Aqueous Extract of RL, i.e., Fe-Ag [3:1] RL*

A mass of RL (2 g) was weighed and washed with distilled water (DW) at ambient temperature. Subsequently, it was immersed into a beaker with 100 mL of boiled DW and stirred for 2 h at 80 °C on a hot plate. The extract solution was filtered twice with a Whatman paper (N°5) to eliminate residual solids. Thereafter, a mass of $AgNO_3$ (50 mg) and a mass of $FeCl_3.6H_2O$ (150 mg), were added respectively into another beaker with 100 mL of filtered RL extract and stirred for 1 h at 60 °C on a hot plate. The pH of the resultant extract was found to be 1.75 with a dark brown color. A mass of NaOH (2 g) was added dropwise into the mixture for a basic medium. The pH of the resultant extract was found to be 11.20 without any change of color. This extract was dried in an oven at 100 °C. After 4 h, a black powder was obtained and thereafter annealed in a ceramic crucible at 800 °C in an open-air furnace for 2 h, leading to a change of color from black to red.

2.2.3 Synthesis of Fe-Ag [7:1] by Gamma Radiolysis Using Co^{60} as Source, i.e., Fe-Ag [7:1] Gamma

A mass of $FeSO_4.7H_2O$ (700 mg) and a mass of $AgNO_3$ (100 mg), were immersed respectively into a beaker with 25 mL of boiled DW and stirred for 30 min at 50 °C on a hot plate. The pH of the resultant solution was found to be 4.53 with an orange color. Thereafter, 10 mL of $CH_3CHOHCH_3$ was added as a scavenger of OH radicals, and a mass of NaOH (75 mg) was added dropwise into the mixture for a basic medium, followed by another 30 min of stirring on a hot plate at 50 °C. The pH of the resultant solution was found to be 10. Two distinct phases were observed (at the top grey color and the bottom black color). The mixture solution was transferred into a test tube for the irradiation process, which was performed after one week. It was exposed to a 50 kGy dose at a dose rate of 50 kGy/min using Co^{60} as the source at ambient temperature. After the irradiation process, the two distinct phases were still observed as the final solution which was centrifuged thrice at 4000 rpm for 20 min with DW and ethanol. Thereafter, it was dried in an oven at 60 °C for 4 h. A black powder was obtained as the final color.

2.3 Analytical Techniques

High-resolution transmission electron microscopy (HRTEM) measurements were performed using a Joel JEM 4000EX electron microscope at an accelerating voltage of 200 kV, equipped with selected area electron diffraction (SAED). Field emission scanning electron microscopy (FESEM) measurements were performed using a Zeiss Ultra 55 scanning electron microscope, equipped with energy-dispersive X-ray spectroscopy (EDS). EDS spectrum was collected with an EDS Oxford instrument with an X-Max solid-state silicon drift detector operated at 20 kV. An X-ray diffractometer, (model Bruker AXS D8 Advance) with an irradiation line Kα1 of copper ($\lambda CuK\alpha 1 = 1.5406$ Å) operating at a voltage of 40 kV and a current of 35 mA, in the angular range of 20 to 90°, was used to study the crystalline nature and structure of the NPs. An attenuated total reflection-Fourier transform infrared (ATR-FTIR) absorption spectrometer (Thermo Nicolet 8700 FTIR spectrometer) was used in the spectral range 400–4000 cm^{-1} to ascertain the surface coating and chemical bonding. The magnetic properties were measured at room temperature using a vibrating sample magnetometer (VSM), (Cryogenic Ltd., UK). Gamma-ray with a Co^{60} source type GIK-9–4, S/N 08,398 and 56 TBq was used.

2.4 Antimicrobial Activities

2.4.1 Microorganisms' Origin, Culture Condition, and Inoculum Preparation

The spoilage organisms used for the study were obtained from the Agricultural Research Council (ARC) Infruitec-Nietvoorbij culture collection (The Fruit, Vine and Wine Institute of the Agricultural Research Council, Stellenbosch, South Africa). From the culture collection, the spoilage yeasts were streaked out on Yeast Malt Peptone Agar (YMA), Glucose (10 g/L), Malt extract (3 g/L), agar bacteriological (20 g/L), Peptone (5 g/L) and incubated at 28 °C until sufficient growth was obtained. From the fully-grown plates containing pure colonies of *Candida guilliermondii*, *Zygosaccharomyces fermentati*, and *Zygosaccharomyces florentinus*. The yeast cultures were further prepared by transferring a wire loop full colony of each yeast into a volume of 5 mL of Yeast Malt broth (YMB) (Sigma Aldrich, SA), and were incubated at 28 °C for 48 h. From each yeast culture broth, the cell concentration was determined by direct count using a Neubauer counting chamber under a microscope at 400 × magnification. As described in the method developed by Mewa-Ngongang et al. [3], a seeding concentration of 10^6 cells/mL in white grape juice agar was used for each of the spoilage yeasts.

Fruit spoilage molds, *Botrytis cinerea*, *Penicillium expansum*, and *Alternaria alstroemeriae*, cultured for 7 to 14 days at 25 °C on potato dextrose agar (PDA, Merck, SA). The spore solutions were prepared by lightly scraping off the surface of the agar with sterile distilled rinsing water. The scrapping off process was done three times to achieve a 100 mL mother spore solution in 250 mL Scott bottles. A 400 × microscopic magnification was used to count the spores from the mother solution, which will allow a preparation of a 10^5 spores/mL solution to be used as inoculum during the growth inhibition assay [9, 10].

2.4.2 Growth Inhibition Assay and Activity Quantification

The growth inhibition method used in this work was adopted from Mewa-Ngongang et al. [3], using grape pomace extract (GPE) agar as a test medium. A mass of 0.2 g of the annealed powders of Fe-Ag [3:1] RL and Fe-Ag [7:1] Gamma, were immobilized in a 100 µL volume of sterile distilled water and were tested against selected spoilage yeasts. From the resulting mixtures, a volume of 10 µL was spotted in 5 mm diameter and 1.7 mm depth wells created on the test agar plates using an agar driller [4, 39]. Before plate inspection for the presence of inhibition zones around the wells, the seeded plates were incubated for 72 h at a temperature of 22 °C. Each sample was tested in three replicates and the average diameter of the zone of inhibition was used for the quantification of growth inhibition activity.

The growth inhibition effect of the best performing (n = 2) NP solutions on mold spore germination was carried out following the aforementioned approach. In three replicates per treatment, the GPE test agar medium was seeded with the corresponding mold spores at the concentration of 10^5 spores/mL. The plates were incubated at 20 °C until a clear zone of inhibition was observed around the 5 mm wells, in which a volume of 10 µL was spotted.

The concept of the volumetric zone of inhibition (VZI) [39] was used to quantify the growth inhibition activity of Fe-Ag [3:1] RL and Fe-Ag [7:1] Gamma solutions against common beverage and fruit spoilage organisms identified, i.e., *C. guilliermondii*, *Z. fermentati*, *Z. florentinus*, *B. cinerea*, *P. expansum*, and *A. alstroemeriae*. The VZI concept expressed in a liter of contaminated solidified media per milliliter of antimicrobial compounds/agents used, i.e., L CSM/mL ACU, is interpreted as the volume of the contaminated medium at a specific cell or spore concentration per milliliter growth-inhibiting solution of Fe-Ag [3:1] RL and Fe-Ag [7:1] Gamma. This method was developed to estimate the amount of NPs or antimicrobial agents required to control spoilage organisms and remove the targeted microbial contamination.

3 Results and Discussion

3.1 Crystallography Analyses

The determination of the crystal structure and purity phase of Fe-Ag NPs were investigated by X-ray diffraction (XRD) analyses as illustrated in Fig. 1.

XRD of Fe-Ag [3:1] RL, generated an Ag/Fe_2O_3 NP profile. The presence of intense and well-defined diffraction peaks of silver (Ag) and hematite (Fe_2O_3) with their maxima centered at 2θ (°) = 24.33, 33.05, 35.45, 38.07, 44.17, 49.19, 53.98, 62.28, 64.46, and 77.32, corresponded to the reflections planes of (012), (104), (110), (111), (200), (024), (116), (214), (220), and (311), indicating the highly crystalline nature of face-centered cubic Ag/Fe_2O_3, the crystallographic reflections of Ag and Fe_2O_3, consistent with the JCPDS patterns No. 004–0783 and No. 033–0664, respectively. The intensive peaks depicted fit the works of Shimpi et al. [29] who synthesized core–shell Ag/Fe_2O_3 NPs using an aqueous extract of *Alstonia scholaris*. By fitting the values to the Scherrer equation, the average size of the particle was found to be 39.59 nm.

XRD of Fe-Ag [7:1] Gamma, generated an Ag/Fe_3O_4 NP profile. The presence of intense and well-defined diffraction peaks of silver (Ag) and magnetite (Fe_3O_4) with their maxima centered at 2θ (°) = 30.03, 35.47, 38.08,

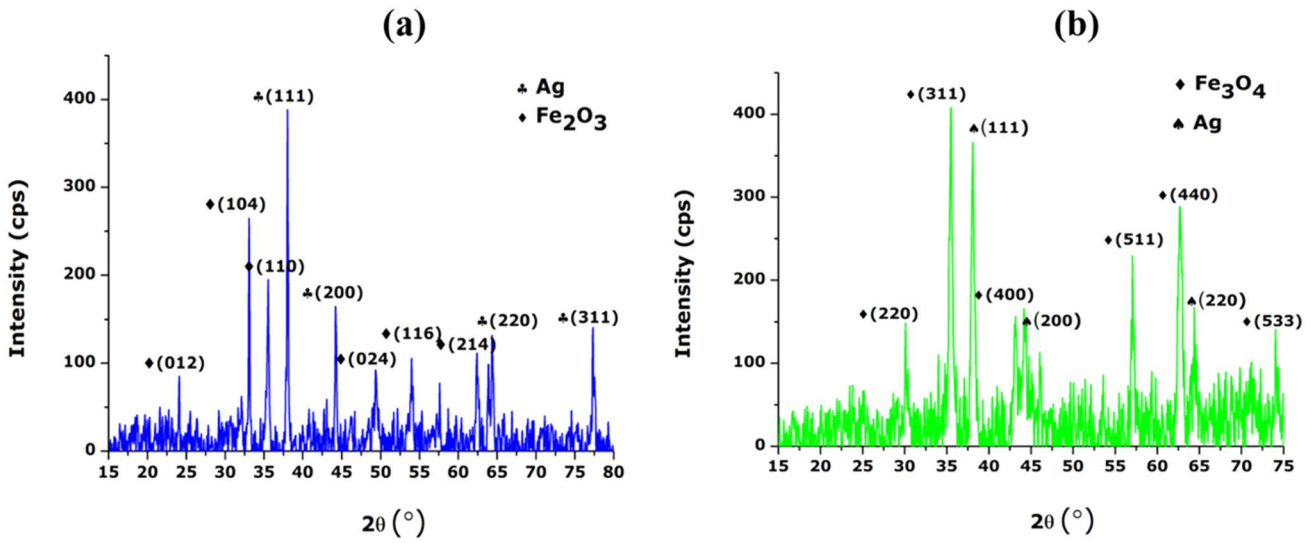

Fig.1 XRD results of **a** Fe-Ag [3:1] RL, and **b** Fe-Ag [7:1] Gamma

42.92, 44.53, 57.21, 62.84, 64.65, and 74.31, matched to the reflections planes of (220), (311), (111), (400), (200), (511), (440), (220), and (533), indicating the highly crystalline nature of the rhombohedral Ag/Fe_3O_4, the crystallographic reflections of Ag and Fe_3O_4, consistent with the JCPDS patterns No. 004–0783 and No. 019–0629, respectively. The intensive peaks presented corroborate with the works of Liu et al. [20] who evaluated the anticancer performance of Ag@Fe_3O_4 NPs. By fitting the values to the Scherrer equation, the average size of the particle was found to be 28.57 nm.

3.2 Microscopic Observations

Figure 2 portrays the shape, size, internal structure, and crystallinity of Fe-Ag NPs from FESEM (Field emission scanning electron microscopy) and HRTEM (High-resolution transmission electron microscopy) micrographs. Well assembled, agglomerated, and crystalline NPs were showcased in both cases with a face-centered cubic structure, spherical shape for Fe-Ag [3:1] RL, and a rhombohedral structure with a cubic shape for Fe-Ag [7:1] Gamma.

Energy-dispersive X-ray spectroscopy (EDS) spectra confirmed the presence of Fe, Ag, and O with some contaminating elements. Selected area electron diffraction (SAED) exhibited multiple diffraction rings with clear diffraction spots demonstrating its polycrystallinity as observed in XRD analyses. By fitting the histogram data with a Gaussian distribution, the average particle size extracted from the HRTEM micrographs was found to be 20.00 ± 0.63 nm for Fe-Ag [3:1] RL and 15.37 ± 0.55 nm for Fe-Ag [7:1] Gamma.

3.3 Vibrational Properties

To validate and confirm the purity of Fe-Ag [3:1] RL and Fe-Ag [7:1] Gamma, attenuated total reflection-Fourier transform infrared spectroscopy (ATR-FTIR) studies were carried out to identify the possible molecules involved in the synthesis as displayed in Fig. 3.

The peaks that appeared around 400 and 500 cm^{-1} were from the skeleton of iron oxide (–O–Fe), and (−O−Ag) stretching vibration mode, respectively which indicated the presence of bimetallic Fe-Ag [14, 17]. The prominent peaks around 800 cm^{-1} were assigned to the FeOOH group. Additionally, the absorption bands around 1000 cm^{-1} were assigned to the C-N of aliphatic amines or alcohols/phenols [37] with absorption bands located around 1300 and 1600 cm^{-1} representing the symmetric and asymmetric bending modes of C = O bonds of amino acid and esters, respectively [30]. Finally, the broad peaks centred approximately around 2000, and 3400 cm^{-1} are associated respectively with standard H_2O bending modes and OH stretching [29].

3.4 Magnetic properties

Figure 4 exhibits the different magnetic properties of Fe-Ag [3:1] RL and Fe-Ag [7:1] Gamma, assessed via a vibrating sample magnetometer (VSM) where the moments in comparison to the applied magnetic field are presented. The temperature of the samples was kept constant at 300 K during the measurement. The applied magnetic field, from the superconducting magnet, varied from − 3 T to + 3 T, while the vibrating amplitude and frequency of the sample

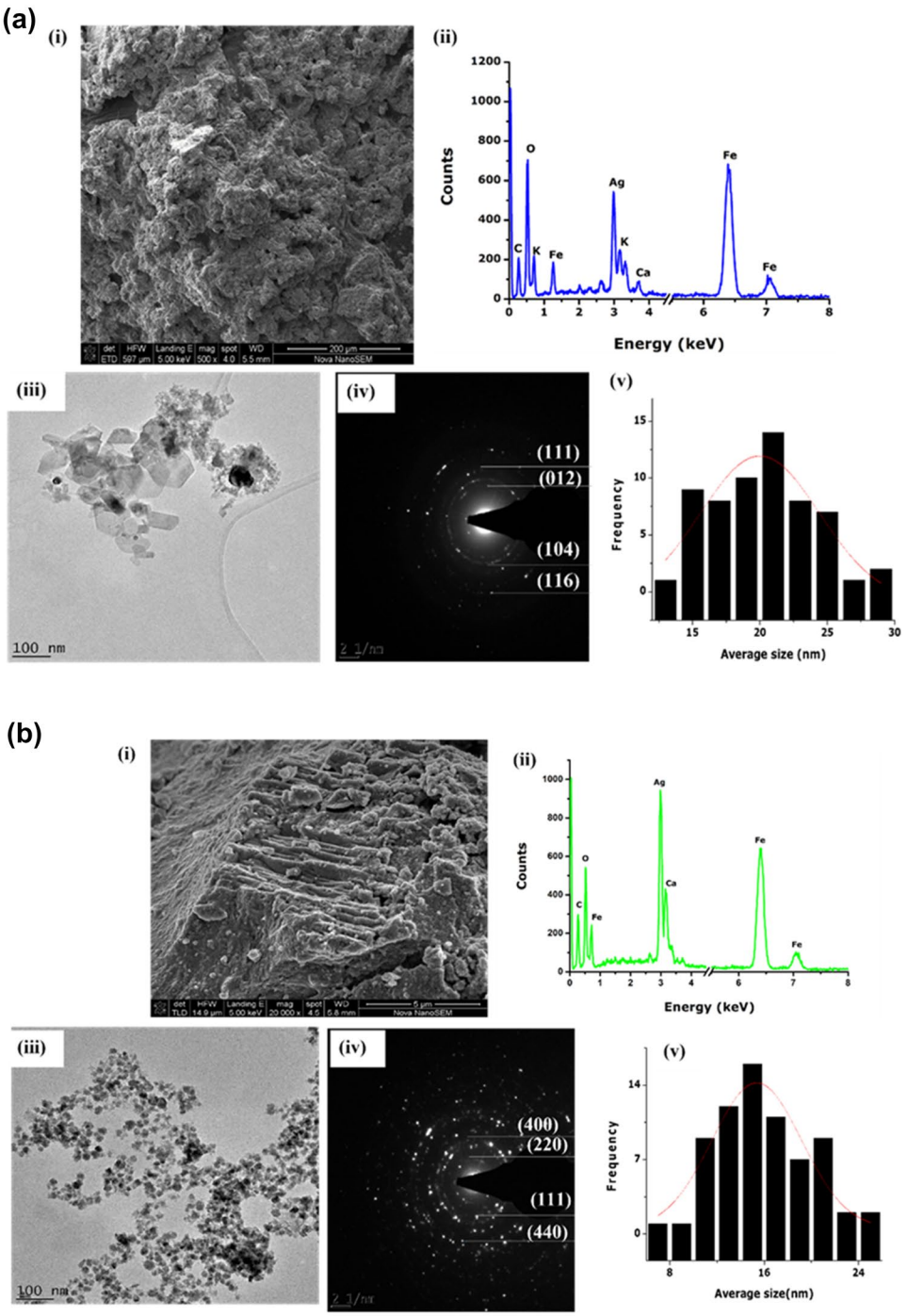

Fig. 2 **(a)** (i) FESEM, (ii) EDS, (iii) HRTEM, (iv) SAED, and (v) average size distribution of Fe-Ag [3:1] RL. **(b)** (i) FESEM, (ii) EDS, (iii) HRTEM, (iv) SAED, and (v) average size distribution of Fe-Ag [7:1] Gamma

holder were set at 0.2 and 20 Hz, respectively. These NPs can be tuned from superparamagnetic to ferromagnetic by modifying the proportion between the Fe and Ag constituents; albeit this is dependent on other parameters including the synthesis method, average size, amount and distribution of cations, annealing temperature, dose rate, and oxygen ion occupancy [19, 40].

3.4.1 Ferromagnetic Behavior

The magnetic hysteresis loops (M-H) suggested a weak ferromagnetic behavior of Fe-Ag [7:1] Gamma, i.e., Ag/Fe_3O_4 NPs. The low value of saturation magnetization ($M_s = 0.0024$ emu/g) compared to bulk values of Fe (218 emu/g), Fe_2O_3 (74 emu/g), and Fe_3O_4 (93 emu/g), confirmed the existence of doping elements as demonstrated by

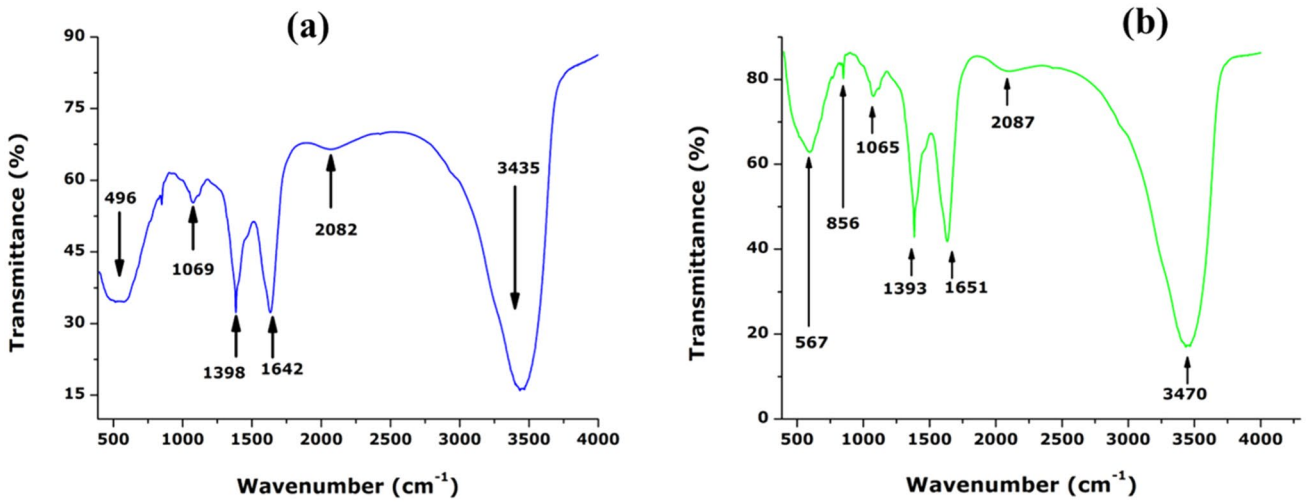

Fig. 3 ATR-FTIR results of **a** Fe-Ag [3:1] RL, and **b** Fe-Ag [7:1] Gamma

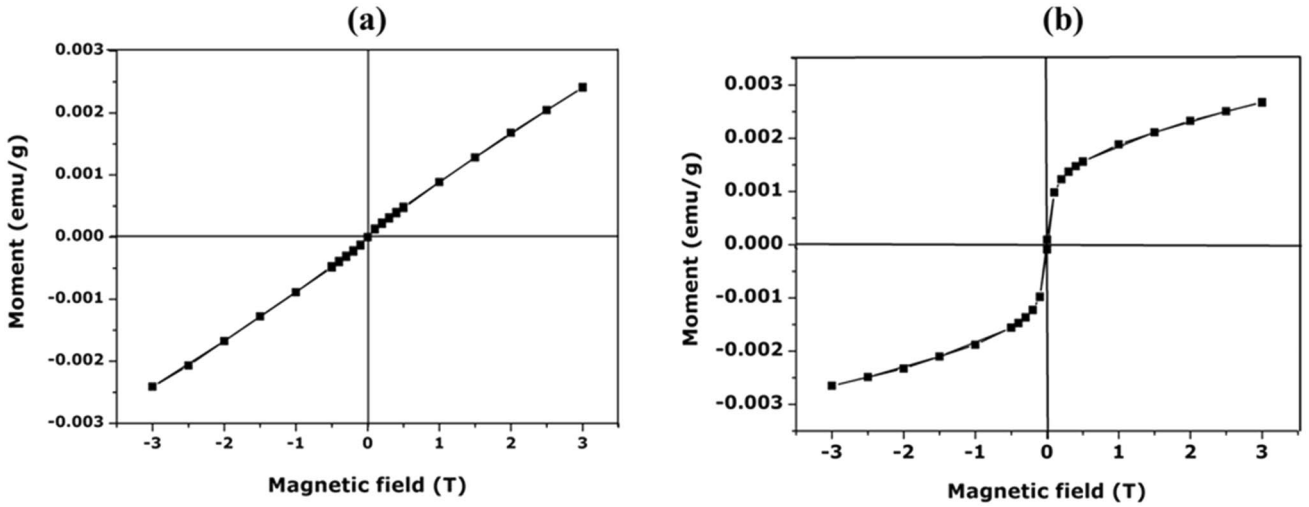

Fig. 4 Magnetic moments of **a** Fe-Ag [7:1] Gamma, **b** Fe-Ag [3:1] RL

XRD and ATR-FTIR analyses. It could be explained by a higher number of defects such as oxygen vacancies at the sample's surface [18]; a decrease in superexchange interaction between iron cations in the tetrahedral and octahedral sites resulting in three important factors such as impurity phases, cationic distribution, surface morphology or size of NPs [41].

3.4.2 Superparamagnetic Behavior

The magnetic hysteresis loops (M-H) of Fe-Ag [3:1] RL, i.e., Ag/Fe_2O_3 NPs, presents a very low coercivity ($H_c = 0.015$ T) close to zero, a very low magnetic remanence ($M_r = 0.0012$ emu/g) and saturation magnetization ($M_s = 0.0026$ emu/g). The drop in the saturation magnetization value of the Ag/Fe_2O_3 NPs may be interpreted as evidence of the effective incorporation of silver metal onto the iron oxide NPs [42]. The magnetic measurements suggested a superparamagnetic behavior of Ag/Fe_2O_3 NPs owing to the reduced coordination symmetry between oxygen atoms at the surface of the NPs, disordered surface spins [43], to the particle size and concentration of the plant extract. The magnetic behavior observed is in line with the works of Mohamed et al. [21] who assessed the magnetic properties of α-Fe/Ag nanocomposites synthesized by a modified polyol route.

Overall, the low coercivity (H_c) accounts for the small value of the magnetocrystalline anisotropy constant (K), which was calculated from the following equation:

$$H_c = \frac{0.98K}{M_s} \quad (1)$$

Furthermore, the value of the squareness (M_r/M_s) was calculated and reported in Table 1. Ag/Fe_2O_3 NPs showed the interaction of NPs by magnetostatic interactions as the squareness < 0.5 [15].

3.5 Antimicrobial Properties

The growth inhibition potential of 20% (m/v) of Fe-Ag [3:1] RL and Fe-Ag [7:1] Gamma, against common beverage and food spoilage yeasts *Z. fermentati*, *C. guilliermondii*, *Z. florentinus* (see Fig. 5) and fruit spoilage molds *B. cinerea*, *P. expansum*, and *A. alstroemeriae* (see Fig. 6), was assessed and the results showed the different levels

Table 1 Magnetic parameters of Fe-Ag [3:1] RL, i.e., Ag/Fe_2O_3 NPs

Magnetic parameters	H_c (T)	M_s (emu/g)	M_r (emu/g)	Squareness (M_r/M_s)	Magnetocrystalline anisotropy constant K (erg/T) × 10^{-5}	Behavior
Ag/Fe_2O_3	0.015	0.0012	0.0026	0.461	3.979	Superparamagnetic

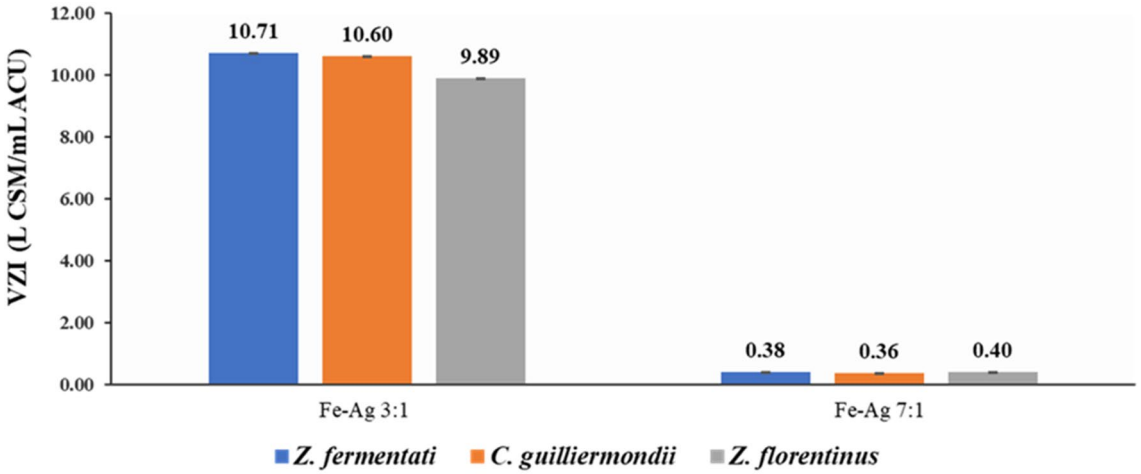

Fig. 5 The histogram showing the growth inhibition activity of 20% (m/v) of Fe-Ag [3:1] RL, Fe-Ag [7:1] Gamma, against *Z. fermentati, C. guilliermondii*, and *Z. florentinus*. VZI in L CSM/mL ACU = Volumetric Zone of Inhibition, expressed in Liter of Contaminated Solidified Media per milliliter of Antimicrobial Compound Used

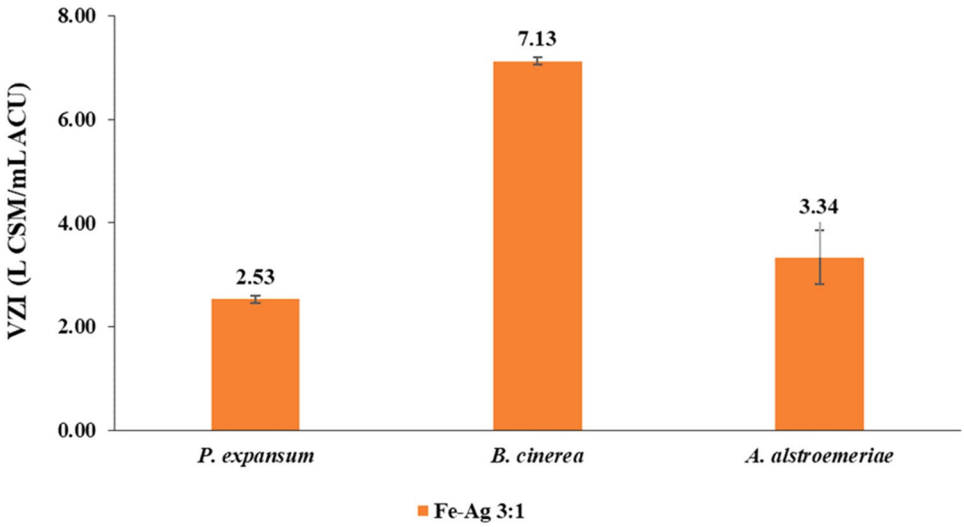

Fig. 6 The histogram showing the growth inhibition activity of 20% (m/v) of Fe-Ag [3:1] RL, against *P. expansum*, *B. cinerea*, and *A. alstromeriae*. VZI in L CSM/mL ACU = Volumetric Zone of Inhibition, expressed in Liter of Contaminated Solidified Media per milliliter of Antimicrobial Compound Used

of growth inhibition activity. In general, the antimicrobial activity of NPs depends on their concentration, size, contact or penetration into microbes' cells. In Fig. 5, Fe-Ag [3:1] RL solution was found to exhibit a higher growth inhibition activity than Fe-Ag [7:1] Gamma. The highest VZI of 10.71 L CSM/ mL ACU suggested that a volume of 1 mL at 20% (m/v) Fe-Ag [3:1] RL solution can suppress the growth of *Z. fermentati* in 10.71 L of contaminated food/beverage at a cell concentration of 10^6 cell/mL. The value of 10.60 is a significant increase in the growth inhibition with a VZI up to × 7.52 higher in comparison with the works of Mewa-Ngongang et al. [3] with C. *guilliermondii*. It is noticeable herein the synthesis method determines the antimicrobial properties of Fe-Ag NPs.

Based on the remarkable antimicrobial activity of Fe-Ag [3:1] RL against spoilage yeasts, this solution was selected for further growth inhibition tests against fruit spoilage molds as illustrated in Fig. 6. The results extended the broad-spectrum of growth inhibition potential, match with the findings of Sameer et al. [34] who reported on better antimicrobial activity of green synthesized Ag@Fe_2O_3 nanocomposites from leaf extract of *Adathoda Vasica*.

These findings report for the first time using the VZI concept, successfully quantifying the biocidal effect of Ag/Fe_2O_3 NPs on the germination of yeast and mold spores expressed in L CSM/mL ACU.

The lowest antimicrobial activity observed with Ag/Fe_3O_4 NPs could be due to its inability to generate enough reactive oxygen species (ROS) which are responsible for growth inhibition of spoilage microorganisms compared to Ag/Fe_2O_3 NPs which portrayed the highest antimicrobial activity with large VZI values. This efficacy might be due to the phenolic compounds prevalent in RL extract which possess excellent antimicrobial properties [44–46], to its shape, size, and composition.

The plausible mechanism is as follows: Ag/Fe_2O_3 NPs and free ions penetrate the microbial surfaces of spoilage yeasts and molds by secreting toxic elements via direct absorption onto biomolecules and generate ROS responsible for oxidative destruction of biological macromolecules including cellular membranes and deoxyribonucleic acid, leading to the capture, degradation, decrease of permeability, and consequently to the death due to the increase of superoxide radicals under visible light exposure [16].

4 Conclusions

For the first time, the synthesis and growth inhibition potential of 20% (m/v) of Fe-Ag [3:1] RL (Ag/Fe_2O_3 NPs) and Fe-Ag [7:1] Gamma (Ag/Fe_3O_4 NPs) by two environmentally salubrious and safe methods, are reported. The characterization techniques revealed different properties from XRD, HRTEM, FESEM, and VSM analyses. The antimicrobial properties revealed the green process was more practical and efficient than the gamma radiolysis, confirming the synthesis method significantly influences the properties of Fe-Ag NPs. This work paves the way to further develop the growth inhibition potential of RL extract-NPs interactions against food and beverage spoilage microorganisms for a broad range of applications in the food and beverage industry, food preservation, to satisfy customers' standards, and multiply innovative food and fruit packaging systems. More so, the efficacy against a large variety of pathogens of rosemary synthesized NPs could be further investigated in subsequent studies for biomedical applications such as antiviral, antioxidant, or anticancer.

Acknowledgements This research program was generously supported by grants from the National Research Foundation of South Africa (NRF), and the Academy of Sciences for the Developing World (TWAS). The authors acknowledge UNESCO-UNISA Africa Chair in Nanosciences & Nanotechnology, iThemba LABS, the Cape Peninsula University of Technology (CPUT), as well as the University of the Western Cape (UWC) to whom they are all grateful.

Author contributions Conceptualization, writing- Original draft preparation: Sandrine Kamdoum Noukelag;Data curation, methodology: Sandrine Kamdoum Noukelag, Maxwell Mewa-Ngongang, Siphelo Ngqoloda, Lebogang Kotsedi;Visualization, investigation: Lovasoa Christine Razanamahandry, Malik Maaza; Writing-review and editing: Sandrine Kamdoum Noukelag, Maxwell Mewa-Ngongang, Seteno K.O. Ntwampe, Christopher J. Arendse; Supervision: Malik Maaza.

Funding National Research Foundation South Africa, UID:139198; North-West University, RK 16; University of the Western Cape, South Africa.

Declarations

Conflict of interest The authors declare no conflict of interest.

References

1. C.A. Monteiro, R.B. Levy, R.M. Claro, I.R. Castro, G. Cannon, A new classification of foods based on the extent and purpose of their processing. Cad Saude Publica **26**(11), 2039–2049 (2010). https://doi.org/10.1590/s0102-311x2010001100005
2. J.M. Zuehlke, B. Petrova, C.G. Edwards, Advances in the control of wine spoilage by *Zygosaccharomyces* and *Dekkera/Brettamoyces*. Annu. Rev. Food Sci. Technol. **4**, 57–58 (2013)
3. M. Mewa-Ngongang, H.W. du Plessis, U.F. Hutchinson, L. Mekuto, S.K.O. Ntwampe, Kinetic modelling and optimization of antimicrobial compound production by *Candida pyralidae* KU736785 for control of *Candida guilliermondii*. Food Sci. Technol. Inter. **23**(4), 1–13 (2017)
4. M. Mewa-Ngongang, H.W. du Plessis, E. Hlangwani, S.K.O. Ntwampe, B.S. Chidi, U.F. Hutchinson, P.N. Neil, Activity interactions of crude biopreservatives against spoilage yeast consortia. Fermentation **5**(3), 53 (2019). https://doi.org/10.3390/fermentation5030053

5. S. Droby, V. Vinokur, B. Weiss, L. Cohen, A. Daus, E.E. Goldschmidt, R. Porat, Induction of resistance to *Penicilium digitatum* in grapefruit by the yeast biocontrol agent *Candida oleophila*. Phytopathology **92**, 393–399 (2002)
6. F. Comitini, N.D. Pietro, L. Zacchi, I. Mannazzu, M. Ciani, *Kluyveromyces phaffii* killer toxin active against wine spoilage yeasts: purification and characterization. Microbiology **150**(8), 2535–2541 (2004)
7. N.N. Mehlomakulu, M.E. Setati, B. Divol, Characterization of novel killer toxins secreted by wine-related non-Saccharomyces yeasts and their action on Brettanomyces spp. Inter. J. Food Microbiol. **188**, 83–91 (2014)
8. C.J. Moir, 2001 Spoilage of processed foods: Causes and diagnosis. The Food Microbiology Group of the Australian Institute of Food Science and Technology Inc., Waterloo, NSW
9. R.R. Sharma, D. Singh, R. Singh, Biological control of postharvest diseases of fruits and vegetables by microbial antagonists: a review. Biol. Control **50**(3), 205–221 (2009)
10. J.I. Pitt, A.D. Hocking, *Fungi and food spoilage*, 3rd edn. (Springer, Boston, 2009), pp.357–382
11. B. Williamson, B. Tudzynski, P. Tudzynski, J.A.V. Kan, Botrytis cinerea: the cause of grey mould disease. Mol. Plant Pathol. **8**(5), 561–580 (2007)
12. M.D. Kirk, S.M. Pires, R.E. Black, M. Caipo, J.A. Crump, B. Devleesschauwer, D. Döpfer, A. Fazil, C.L. Fischer-Walker, T. Hald, A.J. Hall, K.H. Keddy, R.J. Lake, C.F. Lanata, P.R. Torgerson, A.H. Havelaar, F.J. Angulo, World health organization estimates of the global and regional disease burden of 22 foodborne bacterial, protozoal, and viral diseases, 2010: a data synthesis. PLoS Med. **12**(12), e1001921 (2015). https://doi.org/10.1371/journal.pmed.1001921
13. R.K. Yadav, R. Gupta, Impact of chemical food preservatives through local product on human health a review. High Technol. Lett. **27**(6), 767–773 (2021). https://doi.org/10.37896/HTL27.6/3780
14. G. Sharma, N.D. Jasuja, M. Kumar, M.I. Ali, Biological synthesis of silver nanoparticles by cell-free extract of spirulina platensis. J. Nanotechnol. **2015**(4), 1–6 (2015). https://doi.org/10.1155/2015/132675
15. L.Y. Wang, J. Luo, S.Y. Shan, E. Crew, J. Yin, C.J. Zhong, B. Wallek, S.S.S. Wong, Bacterial inactivation using silver-coated magnetic nanoparticles as functional antimicrobial agents. Anal. Chem. **83**, 8688–8695 (2011)
16. Y. Li, W. Zhang, J. Niu, Y. Chen, Mechanism of photogenerated reactive oxygen species and correlation with the antibacterial properties of engineered metal-oxide nanoparticles. ACS Nano **6**(6), 5164–5173 (2012). https://doi.org/10.1021/nn300934k
17. D. Zahra, R. Mojtaba, G. Mostafa, K. Fatemeh, Green synthesis of Ag-Fe3O4 nanocomposite utilizing *Eryngium planum* L. leaf extract and its potential applications in medicine. J. Drug Deliv. Sci. Technol. **67**, 102941 (2022). https://doi.org/10.1016/j.jddst.2021.102941
18. T. Zargar, A. Kermanpur, Effects of hydrothermal process parameters on the physical, magnetic, and thermal properties of $Zn_{0.3}Fe_{2.7}O4$ nanoparticles for magnetic hyperthermia applications. Ceram. Int. **43**(7), 5794–5804 (2017)
19. S. Arokiyaraj, M. Saravanan, N.K.U. Prakash, A.M. Valan, B. Vijayakumar, S. Vincent, Enhanced antibacterial activity of iron oxide magnetic nanoparticles treated with Argemonemexicana L. leaf extract: an in vitro study. Mater. Res. Bull. **48**(9), 3323–3327 (2013)
20. B. Liu, J. Zhou, B. Zhang, J. Qu, Synthesis of Ag@Fe_3O_4 nanoparticles for photothermal treatment of ovarian cancer. J. Nanomater. **2019**, 6457968 (2019). https://doi.org/10.1155/2019/6457968
21. A. Mohamed, R.B. Parvatheeswara, M.O. Abdel-Hamed, K. CheolGi, Modified polyol route for synthesis of Fe_3O_4/Ag and α-Fe/Ag nanocomposite. J. Alloys Compd. **615**, 308–312 (2014)
22. P. Lu, T. Jing, C.Y. Hong, Synthesis of Fe_3O_4, Fe_2O_3, Ag/Fe_3O_4 and Ag/Fe_2O_3 nanoparticles and their electrocatalytic properties. Sci. China Chem. **56**(3), 362–369 (2013). https://doi.org/10.1007/s11426-012-4763-y
23. N. Medina-Córdova, R. López-Aguilar, A.I. Campa-Córdova, C. Angulo, Biocontrol activity of the marine yeast debaryomyces hanseni against phytopathogenic fungi and its ability to inhibit mycotoxins production in maize grain (*Zea mays* L.). Biol. Control. **97**, 70–79 (2016)
24. D.K. Chmielewska, U. Gryczka, W. Migdal, Recent patents on creative ionizing radiation in nanotechnology. Recent Pat. Nanotechnol. **2**(3), 201–207 (2008). https://doi.org/10.2174/1872210087867369615
25. S. Ying, Z. Guan, P.C. Ofoegbu, P. Clubb, C. Rico, F. He, J. Hong, Green synthesis of nanoparticles: current developments and limitations. Environ. Technol. & Innov. **26**, 102336 (2022). https://doi.org/10.1016/j.eti.2022.102336
26. J.F. Hund, M.F. Bertino, G. Zhang, C.S. Levantis, N. Lewantis, A.T. Tokuhiro, J. Farmer, Formation and entrapment of noble metal clusters in silica monoliths by gamma radiolysis. J. Phys. Chem. B **107**, 465–469 (2003)
27. S. Kalunge, A.V. Humbe, M.V. Khedkar, S.D. More, A.P. Keche, A.A. Pandit, Investigation on synthesis, structural and electrical properties of zinc ferrite on gamma irradiation. J. Phys. Conf. series **1644**(1), 012017 (2020). https://doi.org/10.1088/1742-6596/1644/1/012017
28. V. Makarov, A. Love, O. Sinitsyna, S. Makarova, I. Yaminsky, M. Taliansky, N. Kalinina, Green nanotechnologies: synthesis of metal nanoparticles using plants. Acta Naturae **6**(1), 35–44 (2014)
29. N.G. Shimpi, M. Khan, S. Shirole, S. Sonawane, Process optimization for the synthesis of silver (AgNPs), iron oxide (α-Fe_2O_3 NPs) and core-shell (Ag-Fe_2O_3 NPs) nanoparticles using the aqueous extract of alstonia scholaris: a greener approach. The Open Mater. Sci. J. **12**(1), 29–39 (2018). https://doi.org/10.2174/1874088X01812010029
30. L. Wei-Hong, N. Yang, Green and facile synthesis of Ag-Fe_3O_4 nanocomposites using the aqueous extract of Crataegus pinnatifida leaves and their antibacterial performance. Mater. Lett. **162**, 157–160 (2016). https://doi.org/10.1016/j.matlet.2015.09.064
31. R. Sandupatla, A. Dongamanti, R. Koyyati, Antimicrobial and antioxidant activities of phytosynthesized Ag, Fe and bimetallic Fe-Ag nanoparticles using *Passiflora edulis*: A comparative study. Mater. Today: Proceed. **44**(1), 2665–2673 (2021)
32. M. Sajjadi, M. Nasrollahzadeh, S.M. Sajadi, Green synthesis of Ag/Fe_3O_4 nanocomposite using *Euphorbia peplus* Linn leaf extract and evaluation of its catalytic activity. J. Coll. Interface Sci. **497**, 1–13 (2017)
33. H. Muthukumar, S.K. Palanirajan, M.K. Shanmugam, S.N. Gummadi, Plant extract mediated synthesis enhanced the functional properties of silver ferrite nanoparticles over chemical mediated synthesis. Biotechnology **26**, e00469 (2020)
34. K. Sameer, M. Jadhav, P. Raikar, D.A. Barretto, S.K. Vootlac, U.S. Raikar, Green synthesized multifunctional Ag@Fe_2O_3 nanocomposites for effective antibacterial, antifungal, and anticancer properties. New J. Chem. **41**, 9513–9520 (2017)
35. S.R. Batakurki, V. Adimule, M.M. Pai, E. Ahmed, P. Kendrekar, Synthesis of Cs-Ag/Fe_2O_3 Nanoparticles Using *Vitis labrusa* Rachis Extract as Green Hybrid Nanocatalyst for the Reduction of Arylnitro Compounds. Topics in Catal. (2022). https://doi.org/10.1007/s11244-022-01593-7
36. J.R. de Oliveira, S.E.A. Camargo, L.D. de Oliveira, *Rosmarinus officinalis* L. (rosemary) as therapeutic and prophylactic

agent. J. Biomed. Sci. **26**, 5 (2019). https://doi.org/10.1186/s12929-019-0499-8
37. S.K. Noukelag, C.J. Arendse, M. Maaza, Biosynthesis of hematite phase Fe_2O_3 nanoparticles using an aqueous extract of Rosmarinus officinalis leaves. Mater. Today: Proceed. **43**, 3679–3683 (2021)
38. M. Ghaedi, M. Yousefinejad, M. Safarpoor, H.Z. Khafri, M.K. Purkait, Rosmarinus officinalis leaf extract mediated green synthesis of silver nanoparticles and investigation of its antimicrobial properties. J. Ind. Eng. Chem. **31**, 167–172 (2015)
39. M. Mewa-Ngongang, H.W. du Plessis, S.K.O. Ntwampe, B.S. Chidi, U.F. Hutchinson, L. Mekuto, P.J. Neil, Grape Pomace Extracts as Fermentation Medium for the Production of Potential Biopreservation Compounds. Foods **8**(2), 51 (2019). https://doi.org/10.3390/foods8020051
40. M. Hoffmann, V.N. Antonov, L.V. Bekenov, K. Kokko, W. Hergert, A. Ernst, Variation of magnetic properties of Sr_2FeMoO_6 due to oxygen vacancies. J. Phys. Condens. Matter. **30**(30), 305801 (2018). https://doi.org/10.1088/1361-648X/aacb8d
41. A. Akbarzadeh, M. Samiei, S. Davaran, Magnetic nanoparticles: preparation, physical properties, and applications in biomedicine. Nanoscale Res. Lett. **7**(1), 144 (2012). https://doi.org/10.1186/1556-276X-7-144
42. R.M. Khafagy, Synthesis, characterization, magnetic and electrical properties of the novel conductive and magnetic polyaniline/$MgFe_2O_4$ nanocomposite having the core–shell structure. J. Alloys Compd. **509**(41), 9849–9857 (2011)
43. Q. Song, Z.J. Zhang, Shape control and associated magnetic properties of spinel cobalt ferrite nanocrystals. J. Amer. Chem. Soc. **126**(19), 6164–6168 (2004)
44. A.A. Mostafa, A.A. Al-Askar, K.S. Almaary, T.M. Dawoud, E.N. Sholkamy, M.M. Bakri, Antimicrobial activity of some plant extracts against bacterial strains causing food poisoning diseases. Saudi J. Biol. Sci. **25**, 361–366 (2018)
45. S. Moreno, T. Scheyer, C.S. Romano, A.A. Vojnov, Antioxidant and antimicrobial activities of rosemary extracts linked to their polyphenol composition. Free Radical Res. **40**(2), 223–231 (2006)
46. E. Lorenzetti, J.R. Stangarlin, O.J. Kuhn, Antifungal activity of rosemary extract on Macrophomina phaseolina and charcoal rot control in soybean. J. Plant Pathol. **99**(3), 783–786 (2017)